An Eulerian Finite Element Model of the Metal Cutting Process

A. Raczy, W. J. Altenhof, and A. T. Alpas

Department of Mechanical, Automotive, and Materials Engineering
University of Windsor, 401 Sunset Avenue
Windsor, Ontario, Canada, N9B 3P4

Abstract

The Eulerian element formulation was employed in the modeling of the orthogonal metal cutting process of commercial purity copper. The constitutive material models elastic-plastic hydrodynamic and Johnson-Cook, were utilized in modeling the workpiece behavior. The capabilities of each model to replicate the experimental chip geometry, stress and strain distributions, and cutting forces, were investigated. The numerical strain distributions, were in good agreement with the experimental strain distribution. The maximum strains of $\bar{\varepsilon}^p = 8.3$ *and* $\bar{\varepsilon}^p = 5.6$ *for the Johnson-Cook material and hydrodynamic material, respectively, occurred in the tool tip region, and were in good correlation with the experimental strain of* $\bar{\varepsilon}^p = 8.1$ *at this location. The experimental and numerical distributions, all predicted strains of approximately* $\bar{\varepsilon}^p = 3.5$ *to 3.6 beneath the machined surface and adjacent to the rake face. The stress distributions in both of the investigated materials were noticeable different. The Johnson-Cook model showed a stress increase of up to 425 MPa in the primary deformation zone, while the hydrodynamic model predicted increased stresses of 380 MPa in the secondary deformation zone. The hydrodynamic stress distribution was more consistent with experimental findings, which similarly showed a stress increase, up to 360 MPa, in the secondary deformation zone. The maximum stress in the hydrodynamic material (410 MPa) and in the Johnson-Cook material (438 MPa) were located at the tool tip, and showed good correlation to the maximum experimental stress of 422 MPa, also occurring at the tool tip. The sizes of both the primary deformation zone (350* μ*m), and the secondary deformation zone (50* μ*m) predicted by the hydrodynamic and Johnson-Cook material models were in agreement with the experimental observations. The steady state cutting force prediction of the hydrodynamic material was 1332 N, and was within 13% of the experimental findings. The numerical–experimental correlations indicate the Eulerian finite element approach is an effective way of modeling the metal cutting process.*

Introduction

Machining is the process of removing unwanted material from a workpiece, and it is one of the most important manufacturing processes due to the value added to the finished product. Obtaining the desired outcome from a machining operation is difficult due to the many input variables that must be controlled while optimizing the process, including tool and workpiece properties, and operation parameters such as cutting speed (v_c), feed (f), rake angle (α), etc., illustrated in Figure 1. Deformation of a workpiece undergoing machining occurs in three regions including the primary deformation zone (PDZ), the secondary deformation zone (SDZ), and the machined surface (Figure 1); plastic deformation generates heat during tool-workpiece contact, which must be minimal to prolong tool life. Despite advances made in optimizing the cutting process, through both experimental and theoretical approaches, the infinite number of input variables and the complexity of material deformation, makes the outcome of the process difficult to foresee.

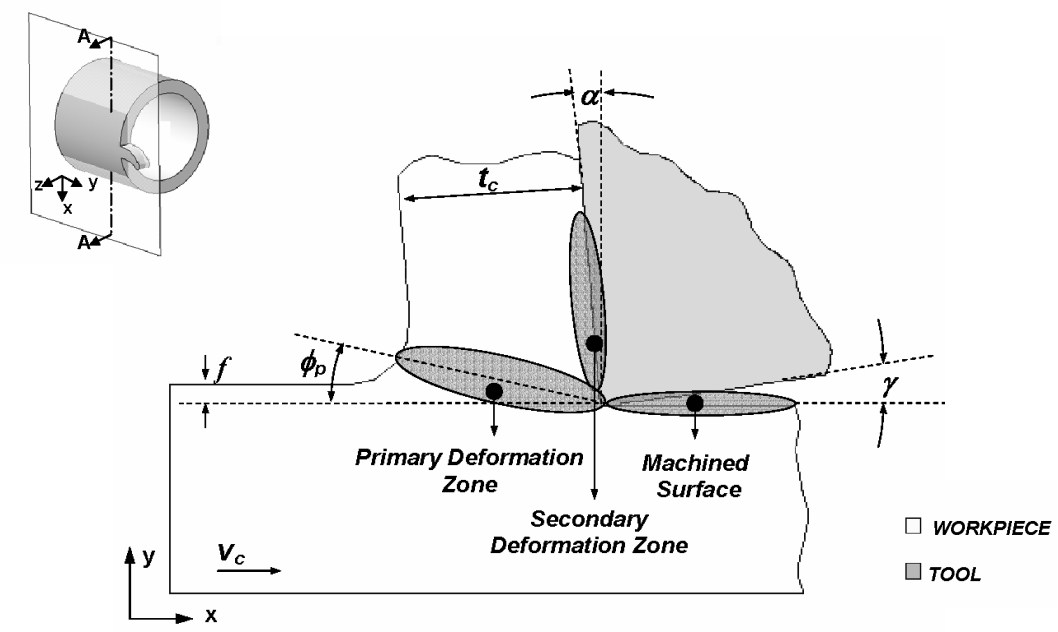

Section A-A

Figure 1: Schematic diagram of deformation zones and cutting parameters labeled on a cross-sectional workpiece undergoing orthogonal cutting, where t_c is the chip thickness, α is the rake angle, γ is the clearance angle, f is the feed, v_c is the cutting speed, and ϕ_p is the primary shear plane angle.

Finite Element (FE) modeling has become an increasingly sought solution to the design of machining operations, since it enables an efficient prediction of material behaviour under various input variable combinations. Majority of the FE models built to simulate the machining process have employed the Lagrangian element formulation [1-5], in which the material is coincident with the element nodal points. As a result of the high strains on the order of 2 to 8 [6] and high strain rates of 10^3 to 10^6 s^{-1} [7] associated with the machining process, the use of a Lagrangian FE mesh is accompanied by severe material and mesh distortion, which degrades the accuracy of the simulation. Common techniques used in preventing mesh distortion involve the use of mesh adaptivity or the application of a failure criterion along a pre-determined line lying parallel to the cutting direction at the level of the tool tip. The use of mesh adaptivity by Ceretti et al. [1], and Marusich and Ortiz [2] has proven to be efficient in eliminating mesh distortion but was costly in computation time. In addition, an inappropriate application of mesh adaptivity criteria may not aid in decreasing error and rather cause excessive processing times. The method of using a failure criterion to enable the separation of neighboring elements at a pre-determined line, can be geometrical and/or physical; the effectiveness of both techniques was investigated by Huang and Black [3]. In the geometrical criteria separation occurs at a critical distance from the tool tip, whereas in the physical criteria separation occurs when a critical shear stress is reached. Combining the geometrical and physical criteria, prompts separation when either the critical distance or critical shear stress is satisfied. The use of a separation criteria has been effectively employed by most researchers, including Zhang and Bagchi [4], and Komvopoulos and Erpenbeck [5]. However, this approach models material fracture rather than the actual behaviour of material deformation.

An alternative method of modeling a workpiece undergoing metal cutting, is to apply an Arbitrary Lagrangian and Eulerian (ALE) or purely Eulerian FE formulations. These

formulations involve a Lagrangian step with an additional advection step, which remaps the mesh deformed during the Lagrangian step to eliminate distortion. The use of Eulerian and ALE element formulations has often been limited to fluid-structure interaction problems such as in Souli et al. [8], and only recently has modeling of solid mechanics problems using an Eulerian FE formulation been explored [9]. Gadala and Wang [10] employed the ALE FE formulation to successfully model metal forming processes such as punching, extrusion, and die forging. As shown by the research of Movahhedy et al. [11], ALE smoothing was insufficient in modeling of the severe material deformation occurring at the tool tip during metal cutting, and as such it was coupled with an Eulerian element formulation.

The objective of this work was to model the deformation behaviour of a commercial purity copper subjected to orthogonal cutting using an Eulerian FE formulation for the workpiece. The application of the Eulerian FE formulation in these simulations provided two significant advantages: (1) the magnitude of strains observed in the machining process were simulated without application of mesh adaptivity, and (2) the use of an Eulerian element formulation eliminated the need to apply an element separation criterion (either physical or geometrical). The model was validated by correlating numerical results to experimentally determined chip thickness, stress distributions, strain distributions and cutting forces, as documented in the research of Elmadagli and Alpas [12].

Development of the Numerical Model

The most significant aspects of the FE model are detailed below, including geometrical discretization, applied boundary conditions, material modeling and contact modeling. All simulations were performed using the explicit non-linear finite element code LS-DYNA, and a personal computer with dual Athlon 1.8 GHz processors with one gigabyte of memory. Explicit time integration was used with a time step size of 6.9 nanoseconds. The termination time ranged between 0.02 and 0.03 seconds, requiring processing time of approximately 120 to 130 hours. The advection method used for the Eulerian workpiece material was a second order Van Leer method [13, 14] to allow the interpolation of properties within an element into a piecewise function.

1. Geometrical Discretization

Three parts were required to model the metal cutting process, namely workpiece, tool and airmesh. A three-dimensional view of the geometry is shown in Figure 2 (a), while Figure 2 (b) shows the cross-sectional view and relevant cutting parameters. The numerical geometry was governed by the experimental set-up [12], in which the rake angle (α) was negative 5 degrees, the clearance angle (γ) was 8 degrees, and the feed (f) was 0.25 mm. In accordance to the illustration in Figure 1, the depth of the model corresponds to the wall thickness of the tubular sample used in the machining experiments which was 3.0 mm. Initially one plane of xy-symmetry was utilized to reduce the model depth to 1.5 mm. Since the feed (0.25 mm) was more then ten time larger then the tube wall thickness (3.0 mm) plain strain conditions were applicable and a second plane of xy-symmetry was applied to simulate infinite wall thickness while further reducing the model depth to 0.27 mm. Material flow was constrained within the two planes of xy-symmetry (Figure 2 (a)), and three elements were used to discretize the workpiece in the z-direction.

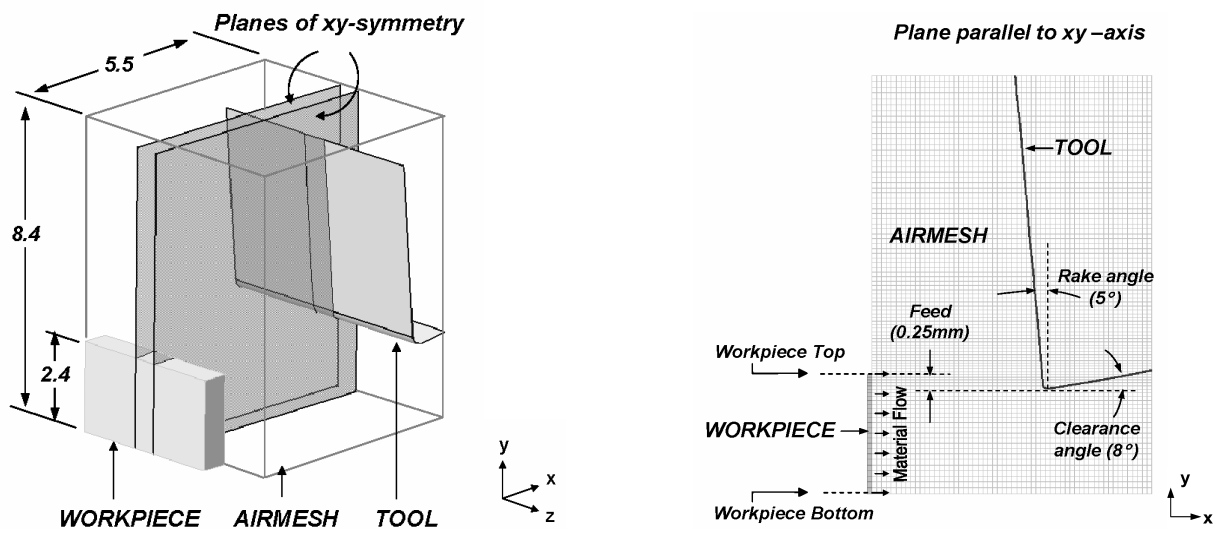

(a) (b)

Figure 2: Geometry of the FE model showing: (a) a three dimensional view of pertinent parts, planes of symmetry, and dimensions in millimeters, and (b) a cross-sectional view of element distribution.

The workpiece was composed of 78 elements characterized as element formulation 12 within LS-DYNA or "single-point integration solid Eulerian elements with single material and void" [15]. In the Eulerian FE formulation the material is not constrained to the original workpiece, therefore an airmesh was constructed to allow the material flowing out of the workpiece mesh to deform throughout the simulation. As the airmesh initially did not contain any material, it was set as a void medium. It was necessary to model this airmesh large enough to provide ample space for any possible material flow, therefore it consisted of 16,008 Eulerian elements of single-point quadrature. As shown in Figure 2 (b), the mesh was refined at the tool tip level where most considerable material displacement occurs, to improve calculation accuracy. The smallest airmesh element dimension in this region was 50 μm. The tool was modeled using Belytschko-Tsay elements of the Lagrangian formulation with refined discretization at the tool tip (smallest shell edge dimension of 60 μm). The radius of the tool tip was modeled as 75 μm, which was consistent with the experimental set-up.

2. Applied Boundary Conditions

In experiments documented by Elmadagli and Alpas [12], the tool was kept stationary while the workpiece was advanced at a surface speed of 600 $mm \cdot s^{-1}$. To properly reflect the experimental set-up, all element nodal point of the tool were restricted from motion in all degrees of freedom and the material of the workpiece was assigned the appropriate velocity through the *BOUNDARY_PRESCRIBED_MOTION keyword command. The elements of the workpiece were classified as ambient with a pressure inflow; this provided a constant flow of material through the workpiece elements and into the airmesh in the direction shown in Figure 2 (b). To ensure that the flow of material remained horizontal throughout the simulation, all nodes along the bottom of the airmesh and workpiece in Figure 2 (b), were restricted to motion only in the x-direction. Material on nodal points of the airmesh and workpiece lying on the xy-planes of symmetry were constrained to move only within the symmetry planes.

3. Workpiece and Tool Material Modeling

The first material type utilized in the defining workpiece behaviour was an elastic plastic hydrodynamic constitutive material model (Material Type 10 within LS-DYNA [16]). Material yielding as a function of equivalent plastic strain ($\sigma = f(\bar{\varepsilon}^p)$) was established through the input of sixteen data points (presented in Table 1), taken from the least-squares fit of a flow curve established experimentally [12]. Figure 3 illustrates the experimental flow curve and the sixteen points used to define the material behaviour in the numerical model.

Equivalent Strain, $\bar{\varepsilon}^p$	Flow Stress, σ (MPa)	Equivalent Strain, $\bar{\varepsilon}^p$	Flow Stress, σ (MPa)
0.0	199.3	4.0	395.4
0.5	251.1	5.0	406.4
1.0	250.9	6.0	415.9
1.5	321.4	7.0	416.7
2.0	344.8	8.0	419.0
2.5	362.8	10.0	421.1
3.0	376.6	15.0	422.1
3.5	387.7	20.0	422.2

Table 1: Equivalent plastic strain and corresponding flow stress values defined for the elastic plastic hydrodynamic material model for ETP copper (C11000).

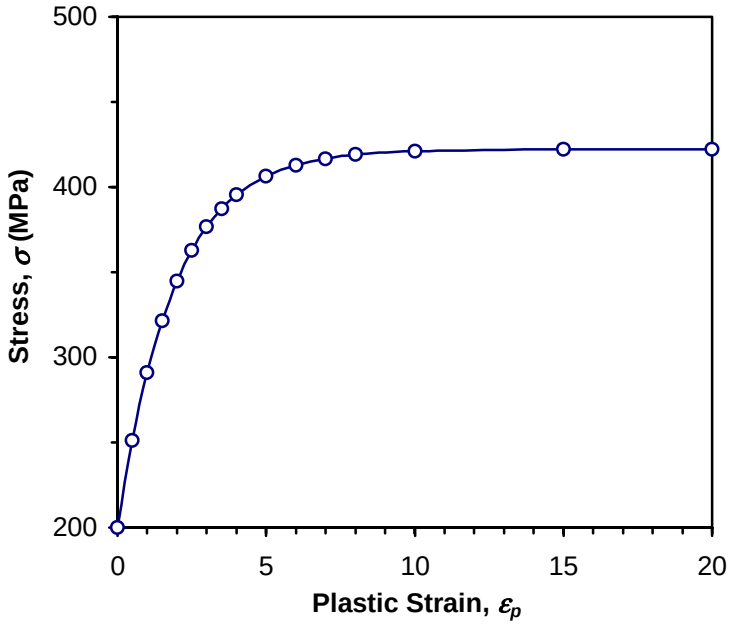

Figure 3: Flow Curve of commercial purity copper obtained from Reference [12], and sixteen points defining the stress-strain behaviour in the hydrodynamic model.

The Johnson-Cook constitutive material model (Material Type 15 within LS-DYNA [16]) was the second material type utilized in the modelling of workpiece behaviour, and defines flow stress as:

$$\sigma = (A + B\bar{\varepsilon}^{p^n})(1 + c\ln\dot{\varepsilon}^*)(1 - T^{*^m}). \quad (1)$$

In Equation 1, $\bar{\varepsilon}^{p}$ is the equivalent plastic strain, $\dot{\varepsilon}^{*}$ is the normalized equivalent strain rate, and T^{*} homologous temperature. The Johnson-Cook constants required to complete the model (*A*, *B*, *n*, *c*, and *m*) were obtained from tests performed by Johnson and Cook [17] on OFHC copper, a material that exhibits properties very similar to those of ETP copper [18]. Table 2 lists constants documented by Johnson and Cook [17] and additional material properties required to complete both of the studied material models.

A (MPa)	*B* (MPa)	*n*	*C*	*m*	ρ (Mg·m^{-3})	*E* (GPa)	ν	T_{melt} (K)
92.0	292.0	0.310	0.025	1.09	8.89	115.0	0.33	1338

Table 2: Properties of ETP copper (C11000) required to complete the Johnson-Cook material model.

Both the hydrodynamic and Johnson-Cook material models utilize a von Mises yield criterion. The equivalent von Mises' stress ($\bar{\sigma}$) is calculated in terms of the deviatoric stress tensor S_{ij} (Equation 2), and the equivalent plastic strain is calculated through time integration of the rate of deformation tensor $D^{p}{}_{ij}$ (Equation 3).

$$\bar{\sigma} = \left(\frac{3}{2} \cdot S_{ij} \cdot S_{ij} \right)^{\frac{1}{2}} \tag{2}$$

$$\bar{\varepsilon}^{p} = \int_{0}^{t} \left(\frac{2}{3} \cdot D^{p}{}_{ij} \cdot D^{p}{}_{ij} \right)^{\frac{1}{2}} dt \tag{3}$$

The Grüneisen equation of state (EOS Type 4 in LS-DYNA [15]) was used to describe the pressure-volume relationship of the copper specimen. Parameters necessary to complete the model were obtained from work by Steinberg [19] and are listed in Table 3.

C_o (cm·μs^{-1})	S_1	S_2	S_3	γ_o	*b*
0.394	1.489	0	0	2.02	0.47

Table 3: Constants required for input in the Grüneisen EOS, for the workpiece material model [19].

Deformation of the tool was negligible in comparison to the workpiece, hence the tool was modelled as a rigid entity (Material Type 20 within LS-DYNA). Properties of the tool material, or SiAlON grade Silicon Nitride, used in the material model were obtained from reference [20] and were specified as follows; the density (ρ = 3.20 Mg·m^{-3}), Young's modulus (*E* = 300.0 GPa), and Poisson's ratio (ν = 0.28). Although Young's modulus is not used to determine the material response of the rigid tool, it is used within the contact algorithm.

4. Coupling of Eulerian Workpiece and Lagrangian Tool

The keyword *CONSTRAINED_LAGRANGE_IN_SOLID was used to model the interaction between the Eulerian workpiece and the Lagrangian tool. The material points of the workpiece were designated as "master"parts, while the "slave" surfaces were those of the tool. Contact coupling was conducted through a 3x3x3 point grid representing virtual nodes associated with the Eulerian workpiece material, which were checked for penetration into the tool.

The keyword command utilized in establishing workpiece-tool contact, enabled the definition of one constant coefficient of friction along the entire contact length. In the hydrodynamic material model it was assumed that the frictional effects were already included within the experimental flow curve and therefore friction in the contact algorithm was neglected (or specified as 0.0). The material behaviour established by Johnson and Cook through standardized mechanical testing methods does not incorporate the effect of external variables such as coefficient of friction; therefore, in the application of the Johnson-Cook material model the effect of the coefficient of friction between the tool and workpiece was taken into account in the contact algorithm. To study the effect of friction on chip formation, the coefficient of friction applied between the tool and workpiece was varied between 0.0 and 0.4.

Numerical Results and Experimental-Numerical Correlation

Progressive chip formation observed in the Eulerian workpiece subjected to metal cutting is shown in Figure 4. The numerical model accurately simulated the nature of chip formation and demonstrated the ability of the Eulerian FE formulation to model the excessive deformation experienced by the workpiece during metal cutting. The illustrated chip formation was the result of preliminary studies, in which only one plane of symmetry and one half of the workpiece depth was modeled. Latter investigations, in which a second plane of symmetry was added, accurately replicated the results of the preliminary investigations in terms of chip formation, strain and stress distribution and cutting forces. Henceforth, two planes of symmetry were applied in simulations to reduce processing time.

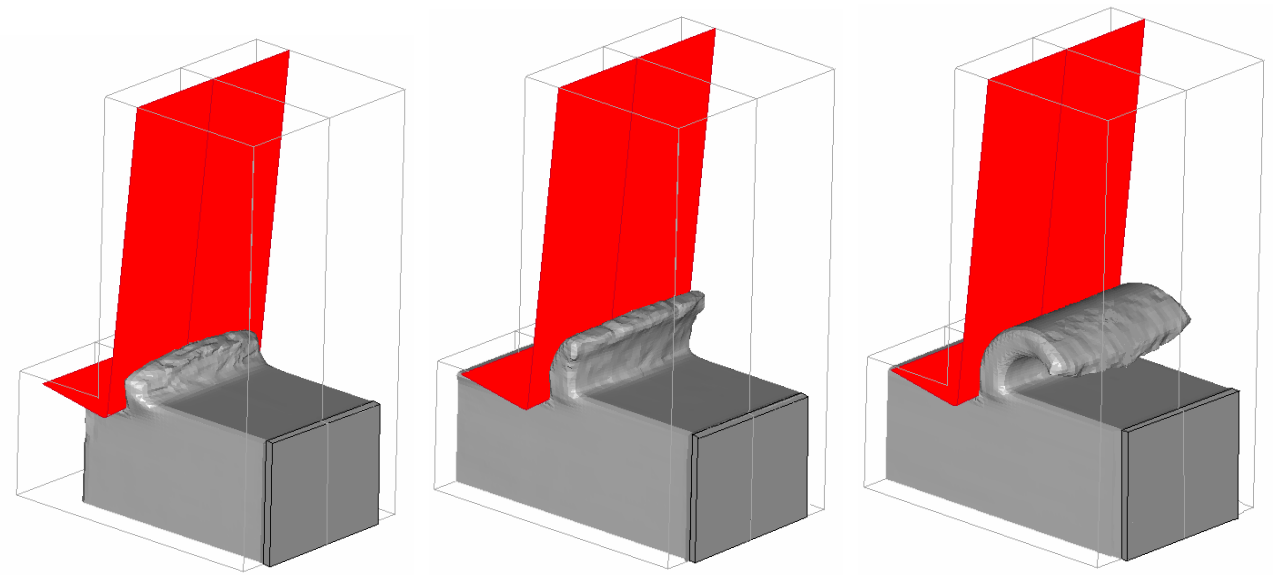

(a) (b) (c)

Figure 4: Chip formation during a metal cutting process, modeled with the Eulerian FE formulation, at times of: (a) 0.0075 seconds, (b) 0.01 seconds, (c) 0.015 seconds.

1. Workpiece Deformation

The chip machined from the hydrodynamic material workpiece and 0.0 friction defined in the contact algorithm, had a thickness of 1.6 mm. The variation of chip thickness with respect to friction applied through the contact definition for the workpiece modeled by the Johnson-Cook material is shown in Figure 5. The chip thickness was found to increase with increasing friction; a chip thickness of 1.05 mm corresponded to friction coefficient of 0.0 and increased to 1.72 mm when friction was increased to a value of 0.4. Ernst and Merchant [21] observed similar increase in chip thickness with progression from a lubricated to dry machining process.

The chip thickness obtained from the experimental workpiece was documented as 1.7 mm, which is in very good agreement with the value observed in the hydrodynamic material despite the fact that friction was not applied in the contact algorithm. This corroborates with the eariler assumption that frictional effects are accoutned for is the experimental flow curve of the hydrodynamic material model. Assuming that the relationship between chip thickness and friction coefficient in the Johnson-Cook material is linear, the expeimental chip thickness of 1.7 mm can be replicated by setting μ=0.39 in the contact algorithm; this was confirmed by performing an additional simulation where the friction coefficient was set to 0.39 and resulting chip geometry was indeed 1.7 mm. The obvious advantage of the hydrodynamic material is that friction does not have to be manipulated to obtain an accurate chip thickness prediction.

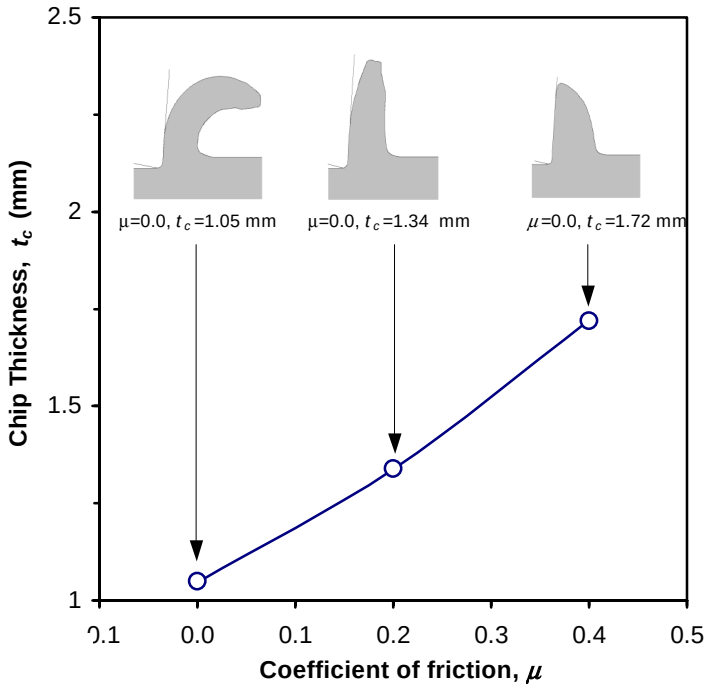

Figure 5: Variation of chip thickness (t_c) with respect to the coefficient of friction applied at the chip-tool interface (μ) for workpiece modeled by the Johnson-Cook material.

2. Strain Distribution

The strain distribution in the material ahead of the tool tip modeled by the hydrodynamic and Johnson-Cook materials is shown in Figure 6 (a) and Figure 6 (b), respectively. The strain distribution of the Johnson-Cook material corresponds to a friction coefficient of 0.39, which best replicated the experimental chip geometry. Trends observed in the strain accumulated by both materials are very similar, with an increase in strain observed at the machined surface and the SDZ. The maximum strain in the machined surface for the hydrodynamic material was 3.5,

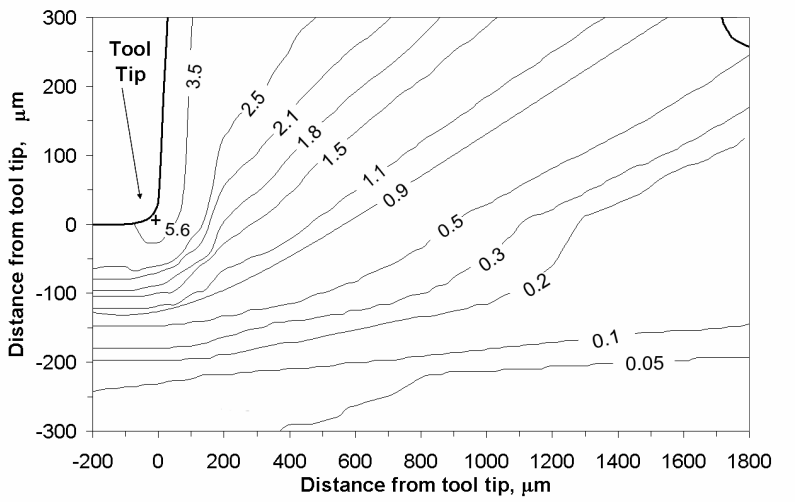

(a)

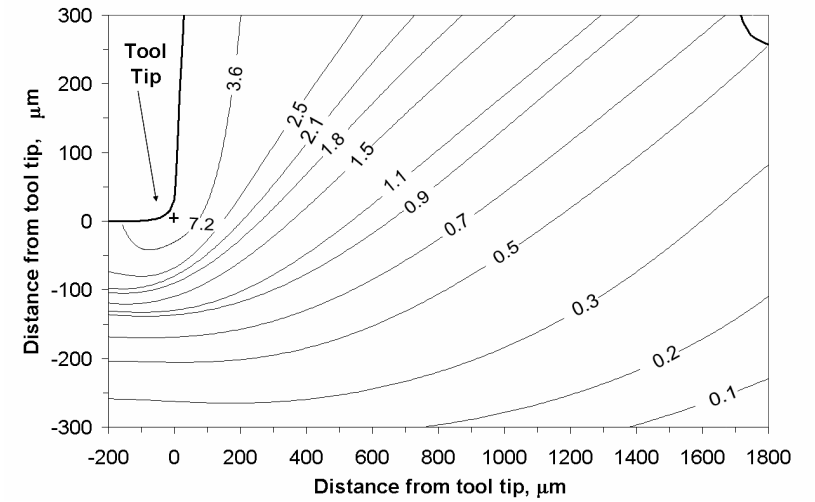

(b)

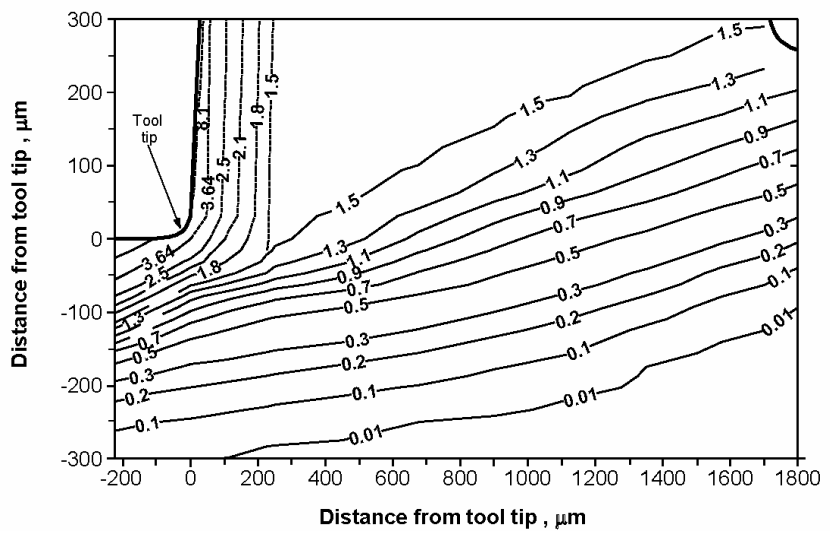

(c)

Figure 6: Distribution of plastic strain in the material ahead of the tool tip according to:
(a) hydrodynamic material model, (b) Johnson-Cook material model, and (c) experimental investigations [12].

slightly lower then 3.6 predicted by the other material. The strain decreased with increasing distance from the cutting line and at depth of 300 μm below the cutting line the strain in the Johnson-Cook material ($\bar{\varepsilon}^p = 0.25$) was higher the then that in the hydrodynamic material ($\bar{\varepsilon}^p = 0.025$). The maximum strain of $\bar{\varepsilon}^p = 5.6$ in the hydrodynamic material occurred at the tool tip, while the Johnson-Cook material had a maximum strain of $\bar{\varepsilon}^p = 8.3$, which occurred slightly above the tool tip. The width of the SDZ in the Johnson-Cook material was wider (at approximately 80 μm) then that of the hydrodynamic material, which was 60 μm. Beyond the SDZ, the strain within the chip ranged between $\bar{\varepsilon}^p = 1.5$ and 2.5 for both material models. Along the PDZ, the strains in both material models decreased from a maximum at the tool tip to a minimum chip root.

The experimental strain distribution was obtained from work of Elmadagli and Alpas [12] and is shown in Figure 6 (c). The trends observed in the SDZ, PDZ and machined surface are consistent with those observed in the numerical models and discussed in the above paragraph. The experimental strains increased at the machined surface and in the SDZ adjacent to the rake face. Maximum experimental strain of approximately $\bar{\varepsilon}^p = 8.1$ occurred slightly above the tool tip along the rake face and was within 2 % of the strain observed in the Johnson-Cook material. The width of the experimental SDZ was approximately 50 μm, which is more accurately predicted by the hydrodynamic model. The experimental strain in the chip was approximately $\bar{\varepsilon}^p = 1.5$, which is similar to the chip strains attained in the numerical results. Although the strain along the PDZ increased from the tool tip to the chip root in both the experimental and numerical results, the strain gradient within the PDZ of the experimental strain distribution was much smaller then that observed in the numerical results. The strain in the machined surface of the experimental results agreed well with both numerical models at depths of 50 μm where $\bar{\varepsilon}^p = 3.5$. At 300 μm, the experimental strain was approximately 0.05 and plastic deformation extended to 400 μm beneath the cutting line; the hydrodynamic material model best replicated these results.

In general, correlation between strain values for the numerical and experimental test methods showed that the trends in the machined surface, SDZ, and PDZ, were in good agreement. The hydrodynamic material model showed the least accuracy in predicting the location of maximum strain, but was otherwise well capable of replicating experimental strains. The Johnson-Cook material exhibited superior agreement with the experimental strain distribution.

3. Stress Distribution

The numerical prediction of von Mises stress distributions in the hydrodynamic material is shown in Figures 7 (a). The stress state in Figure 7 (b) corresponds to the Johnson-Cook material with contact friction defined as 0.39, to replicate the conditions during experimental machining tests. The stress distributions obtained through numerical simulation of the two studied material models varied significantly. The hydrodynamic material demonstrated an increase in stress at the machined surface and in the SDZ adjacent to the rake face, similar to trends observed in strain distributions. The Johnson-Cook material model showed an increase in stress within the PDZ but a decrease in stress at the tool rake face in the SDZ. The maximum stresses for both models were located at the tool tip; they were 410 MPa for the hydrodynamic material and 438 MPa for the Johnson-Cook material. Along the PDZ of the hydrodynamic material, the stresses decreased from a maximum at the tool tip to a minimum of 260 MPa at the

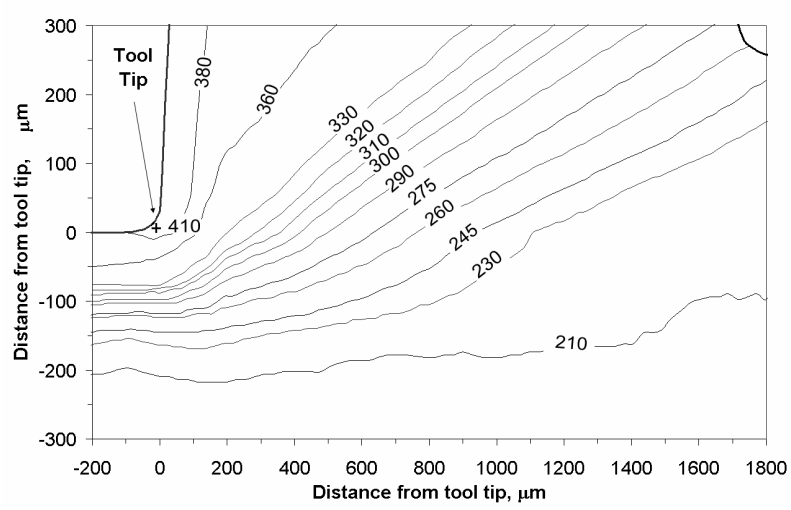

(a)

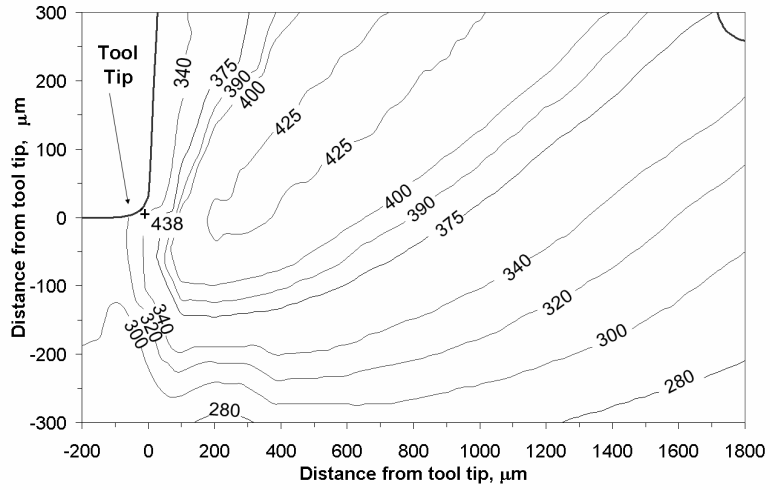

(b)

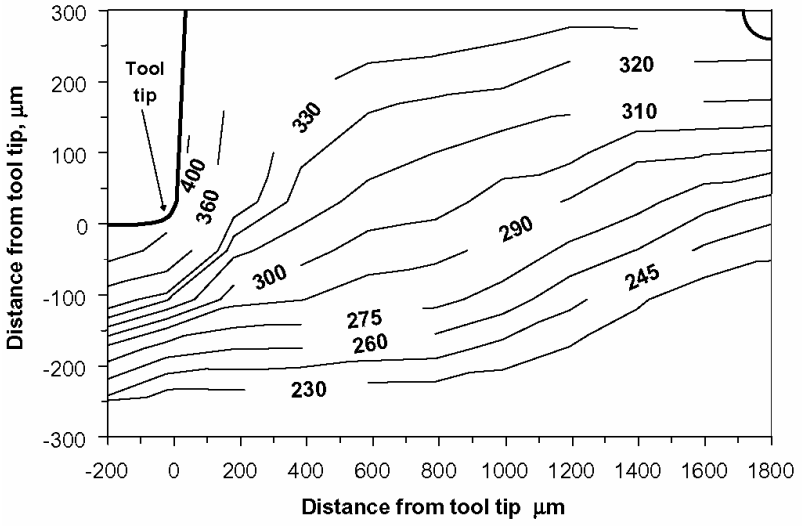

(c)

Figure 7: Distribution of stress in the material ahead of the tool tip, in units of MPa, according to: (a) hydrodynamic material model, (b) Johnson-Cook material model, and (c) experimental investigations [12].

chip root, whereas the stress in the PDZ of the Johnson-Cook material remained approximately constant at 400-425 MPa. In the SDZ of the hydrodynamic material model the stress was maximum adjacent to the tool rake face (380 MPa) and decreased towards the free surface of the chip. The stress at the rake face in the Johnson-Cook material was as low as 340 MPa and increased with increasing distance from the rake face. The numerical models both predicted a decrease in stress with increasing depth below the cutting line beneath the machined surface. These stresses were much higher in the machined surface of the hydrodynamic material (360 MPa) than in the Johnson-Cook material (300 MPa). Stresses above the yield strength were contained within regions where plastic strain was detected, as dictated by the constitutive material models.

For the purpose of numerical-experimental correlation, Figure 7 (c) shows the experimental stress distribution generated from information provided in reference [12]. The experimental stress distribution showed trends agreeing with those present in the hydrodynamic material, where stresses increased in the SDZ and the machined surface. The maximum stress values in the machined surface and SDZ of the hydrodynamic material varied from the experimental results by only 5 % and 10 %, respectively. The stress decrease at the rake face of the Johnson-Cook material was inconsistent with the experimental results, while the maximum stresses in the machined surface varied by 17 % from the experimental. The absolute maximum stress value in the experimental workpiece was 422 MPa located at the tool tip, which was in good agreement with both numerical models. The experimental stress along the PDZ increased from a maximum at the tool tip to a minimum at the chip root, much like in the hydrodynamic material. The width of the PDZ was estimated to be approximately 350 μm for all three presented stress distributions; in the hydrodynamic and experimental results the PDZ width was measured between the 230 MPa and 330 MPa stress contour, while the PDZ of the Johnson-Cook material was contained in the 400 MPa stress contour. The hydrodynamic material in general best replicated the experimental stress distribution. A probable cause of the poor stress distribution predictions of the Johnson-Cook material model was the consideration of strain rate effects paired with omission of the thermal softening influence; these should be considered simultaneously to create a dynamic equilibrium between work hardening and the recovery process.

4. Cutting Force

The cutting force (or the x-force) was monitored throughout the simulation of both material models studied, and is shown in Figure 8. The force remained zero until the workpiece and tool came into contact, which occurred at approximately 0.005 seconds. Simulation performed with the hydrodynamic material was terminated at a time of 0.03 seconds, with the cutting force equal to 1332 N. The Johnson-Cook material simulation with μ=0.39 was terminated at 0.02 seconds resulting in a cutting force value of 1970 N. At the designated termination time of each simulation, the cutting force was still slightly increasing but since the chip thickness, stress distributions, and strain distributions had all reached steady state, the cutting force at this time was also considered as steady state. In addition to time, the coefficient of friction was a variable in the investigation of the Johnson-Cook material and enabled the study of its effect on the cutting force, which is summarized in Figure 9. Increasing friction at the tool-workpiece interface increased the cutting force generated during the operation.

The experimental cutting force (dashed line in Figure 8) had a steady state value of 1177 N. The hydrodynamic material model best predicted this force, with an overestimation of only 13 %. The Johnson-Cook material with μ=0.39 overestimated the experimental cutting force by 21 %.

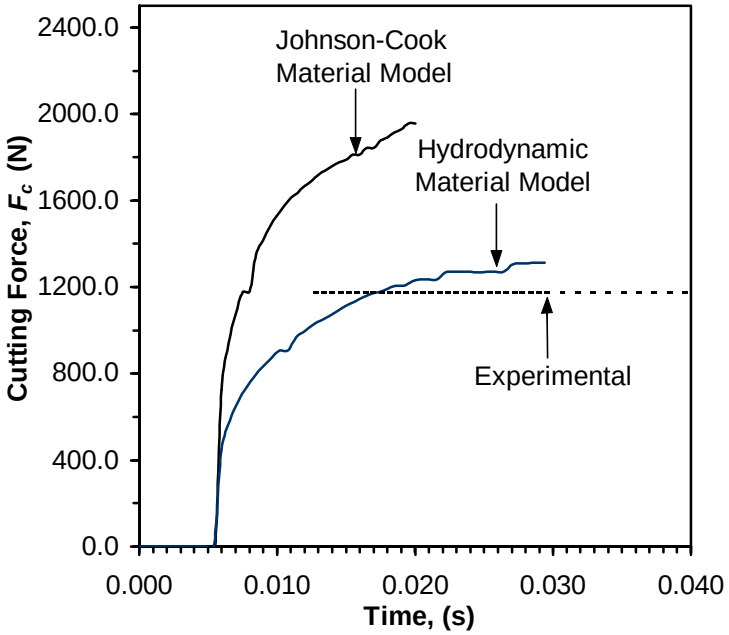

Figure 8: Cutting force (F_c), in units of N, for both studied material models and the steady state cutting force for the machining tests [12].

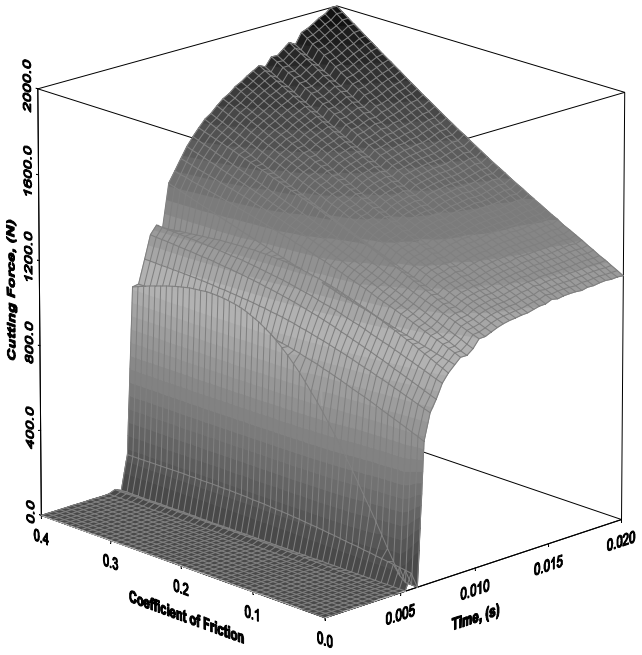

Figure 9: Surface plot of cutting force (F_c) variation in the Johnson-Cook material, in units of N, with respect to time and friction.

Conclusions

An Eulerian FE formulation was employed in modeling of the metal cutting process. Two material models namely, an elastic plastic hydrodynamic and Johnson-Cook constitutive model, were used to predict the stress distribution, strain distribution and cutting forces arising in the material ahead of the tool tip in commercial purity copper sample undergoing chip formation. The numerical findings were correlated to experimental results to validate the developed FE model. Overall, the hydrodynamic material model was more accurate in its predictions of stress distribution and cutting force, while still adequately predicting the strain distribution. The most significant inaccuracy of the Johnson-Cook material was found in its prediction of the stress state in the material. Correlations drawn from the comparison of experimental finding and the superior numerical model, or the hydrodynamic material model, are as follows.

1. The hydrodynamic material was able to replicate the experimental chip thickness of 1.7 mm with a 5 % error, without the manipulation of the friction coefficient in the contact algorithm.
2. The numerical strains of $\bar{\varepsilon}^p = 5.6$ predicted for the tool tip was also the maximum stain accumulated in the workpiece. The maximum strain in the experimental findings was located slightly above the tool tip and had a value of $\bar{\varepsilon}^p = 8.1$. Numerically determined strains 50 μm ahead of the tool tip and 50 μm below the cutting line were $\bar{\varepsilon}^p = 3.5$, which compared well with $\bar{\varepsilon}^p = 3.64$ calculated experimentally for the same locations. The depth of plastic deformation beneath the machined surface (400 μm) and the width of the SDZ (60 μm) predicted by the numerical model were in good agreement with experimental observations. Experimentally, the strain in the chip reached values of $\bar{\varepsilon}^p = 1.5$, while numerically the strain in the chip ranged from $\bar{\varepsilon}^p = 1.8$ to 2.5.
3. The maximum von Mises stress of 410 MPa predicted by the hydrodynamic material model occurred directly ahead the tool tip, which corresponded well with the location and stress value found through experimental investigations. In the SDZ, the highest experimentally estimated stress value was 360 MPa, which was in agreement with the numerically predicted value of 380 MPa. Strains calculated both numerically and experimentally were found to decrease: along the PDZ (traveling from tool tip to chip root), with increasing distance from the rake face, and with increasing depth below the cutting line. Approximate PDZ width in the hydrodynamic model was consistent with the PDZ width in experimental results.
4. The cutting force calculated numerically using the hydrodynamic material to model the workpiece (1332 N), predicted the experimental cutting force of 1177 N with 13 % error.

References

1. Ceretti, E., Fallbohmer, P., Wu, W.T. and Altan T.R., “Application of 2D FEM to Chip Formation in Orthogonal Cutting”, p. 169-180, Journal of Materials Processing Technology (1996).
2. Marusich, T.D. and Ortiz, M., “Modelling and Simulation of High-Speed Machining”, p. 3675-3694, International Journal for Numerical Methods in Engineering (1995).
3. Huang, J.M. and Black, J.T., “An Evaluation of Chip Separation Criteria for the FEM Simulation of Machining”, p. 545-554, Journal of Manufacturing Science and Engineering (1996).
4. Zhang, B. and Bagchi, A., “Finite Element Simulation of Chip Formation and Comparison with Machining Experiment”, p. 289-297, Journal of Engineering for Industry (1995).
5. Komvopoulos, K. and Erpenbeck, S.A., “Finite Element Modeling of Orthogonal Metal Cutting ”, p. 253-267, Journal of Engineering for Industry (1991).
6. Von Turkovich, B.F., “Shear Stress in Metal Cutting”, p. 151-157, Journal of Engineering for Industry (1970).

7. Stevenson, M.G. and Oxley, P.L.B., "Measuring Stress/Strain Properties at Very High Strain Rates Using a Machining Test", p. 308-313, Journal of the Institute of Metals (1967).
8. Souli, M., Ouahsine, A. and Lewin, A., "ALE Formulation for Fluid-Structure Interaction Problems", p. 659-675, Computer Methods in Applied Mechanics and Engineering (2000).
9. Belytschko, T., Liu, W.K. and Moran, B., "Nonlinear Finite Elements for Continua and Structures", John Wiley and Sons Ltd., West Sussex, England (2000).
10. Gadala, M.S. and Wang, J., "ALE Formulation and its Application in Solid Mechanics", p. 33-55, Computer Methods in Applied Mechanics and Engineering (1998).
11. Movahhedy, M., Gadala M.S. and Altintas Y., "Simulation of the Orthogonal Metal Cutting Process using an Arbitrary Lagrangian-Eulerian Finite-Element Method", p. 267-275, Journal of Materials Processing Technology (2000).
12. Elmadagli, M. and Alpas, A.T., "Metallographic analysis of the deformation microstructure of copper subjected to orthogonal cutting", p. 249-259, Materials Science and Engineering A, (2003).
13. Van Leer, B. "Towards the Ultimate Conservative Difference Scheme: IV. A New Approach to Numerical Convection", p. 276-299, Journal of Computational Physics (1977).
14. Van Leer, B., "Towards the Ultimate Conservative Difference Scheme: II. Monotonicity and Conservation Combined in a Second-Order Scheme", p. 361-370, Journal of Computational Physics (1973).
15. "LS-DYNA 970 Keyword User's Manual Volume I", Livermore Software Technology Corporation, Livermore, CA (2003).
16. "LS-DYNA 970 Keyword User's Manual Volume II", Livermore Software Technology Corporation, Livermore, CA (2003).
17. Johnson, G.R. and Cook, W.H., "A Constitutive model and data for metals subjected to large strains, high strain rates and high temperatures", p. 541-547, Proceedings from the 7th International Symposium on Ballistics, The Hague, The Netherlands (1983).
18. ASM International, "Metals Handbook: Volume 2", ASM International, Metals Park, OH (1979).
19. Steinberg, D., "Equation of State and Strength Properties of Selected Materials", Lawrence Livermore National Laboratory, Livermore, CA (1996).
20. ASM International, "Metals Handbook: Volume 16", ASM International, Metals Park, OH (1989).
21. Ernst, H. and Merchant, M.E., "Surface Friction of Clean Metals: A Basic Factor in the Metal Cutting Process", p. 76-101, Proceedings of the special summer conferences on Friction and Surface Finish, The M.I.T. Press, Cambridge, MA (1940).